Biomedical Signal Processing and Control 89 (2024) 105795

Contents lists available at ScienceDirect

Biomedical Signal Processing and Control

journal homepage: www.elsevier.com/locate/bspc

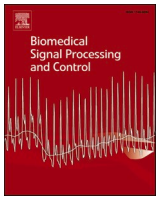

Recurrence quantification analysis of uterine vectormyometriogram to identify pregnant women with threatened preterm labor

Felix Nieto-del-Amor [a], Gema Prats-Boluda [a,*], Wanting Li [b], Jose L. Martinez-de-Juan [a], Lin Yang [b], Yongxiu Yang [b], Dongmei Hao [b], Yiyao Ye-Lin [a]

[a] Centro de Investigación e Innovación en Bioingeniería, Universitat Politècnica de València, 46022 Valencia, Spain
[b] Faculty of Environment and Life, Beijing University of Technology, Beijing International Science and Technology Cooperation Base for Intelligent Physiological Measurement and Clinical Transformation, Beijing 100124, China

ARTICLE INFO

Keywords:
Preterm labor
Vectormyometriogram
RQA
Recurrence plot, electrohysterography

ABSTRACT

Electrohysterography has been shown to provide relevant information on preventing preterm labor. Recent studies have confirmed the feasibility of using the vectormyometriogram (VMG) to assess uterine myoelectric vector displacement, with different physiological implications for the slow and fast waves, without suggesting its implementation in clinical practice. The fast wave VMG component has dynamic behavior in any specific direction on the X-Y plane. Since recurrence is a common feature of dynamic systems, we aimed to determine the recurrence pattern of uterine vector displacement, exploring its clinical potential in detecting imminent and preterm labor in women with threatened preterm labor and a serious preterm birth risk. For this, we analyzed the recurrence patterns from a 2D-vectormyometriogram using four common statistics: determinism, longest diagonal, entropy, and laminarity. We found significantly increased determinism (0.035 ± 0.011 vs. 0.077 ± 0.041), entropy (1.768 ± 0.116 vs. 2.197 ± 0.24) and laminarity (0.086 ± 0.034 vs. 0.173 ± 0.078) from the early (26–30 weeks) to late (35–37 weeks) gestation stages. As pregnancy progresses, the uterine vector displacement becomes more periodic, predictable and stable, while VMG recurrence statistics in the fast wave high bandwidth better detect imminent and preterm labor, outperforming classical EHG parameters from bipolar channels. The proposed method was also resistant to motion artifacts and preserved its discriminative capacity between the groups. Our results on VMG recurrence statistics could thus be another reliable biomarker for preventing preterm labor in women with threatened preterm labor and would favor transferring the EHG technique to clinical practice.

1. Introduction

Preterm birth is defined as births before the 37th week of gestation, form approximately 11 % of all births [1] and affects around 15 million families worldwide [1]. Premature births are responsible for 1 million neonatal deaths annually and are the leading cause of neonatal mortality in the first four weeks of life [2]. The babies that survive are associated with 1 in 5 mental retardations, 1 in 2 cerebral palsies, and 1 in 3 eye injuries [2]. Premature babies are also at risk of other long-term morbidities, such as asthma, learning disabilities, attention deficit disorder and emotional problem [3]. Preterm birth health care requires a significant drain on hospital resources. In the U.S., the gross annual economic burden attributed to preterm delivery in 2016 was $25.2 billion relative to term or post-term births, more than $64815 per premature baby [4].

Threatened preterm labor (TPL), which occurs in approximately 9 % of all pregnancies, is a leading risk factor for preterm birth and the most common cause of hospitalization admission in the second half of pregnancy [5]. TPL is associated with significant maternal morbidity, prolonged patient admission periods and a substantial expenditure of health care resources [6]. The economic burden related to TPL was estimated at $820 million per year in the U.S. [7]. The average cost of a 'false' TPL was estimated to be $20,372 per patient [8]. TPL may also involve more or less aggressive treatments with possible side effects, significant distress for the pregnant woman and her family and reduced attention to other children in the family. 75–95 % of women with TPL do not deliver

* Corresponding author.
E-mail addresses: feniede@ci2b.upv.es (F. Nieto-del-Amor), gprats@ci2b.upv.es (G. Prats-Boluda), liwanting@emails.bjut.edu.cn (W. Li), jlmartinez@ci2b.upv.es (J.L. Martinez-de-Juan), yanglin@bjut.edu.cn (L. Yang), yyx14323@emails.bjut.edu.cn (Y. Yang), haodongmei@bjut.edu.cn (D. Hao), yiye@ci2b.upv.es (Y. Ye-Lin).

https://doi.org/10.1016/j.bspc.2023.105795
Received 18 May 2023; Received in revised form 19 September 2023; Accepted 25 November 2023
Available online 28 November 2023

Table 1
Demographic description of the dataset (median (IQR Q1–Q3)).

	Imminent	Non-imminent	*p*-value
Sample size	17	38	–
Week of gestation	35.6 (IQR 33.3–36.3)	31.4 (IQR 29.4–32.7)	<0.001
Week of labor	35.7 (IQR 33.3–36.6)	38.6 (IQR 37.2–39.9)	<0.001
Parity	0 (IQR 0–1)	0 (IQR 0–0)	N.S.
Maternal age (years)	32 (IQR 29–36)	32 (IQR 30–35)	N.S.
	Preterm	**Term**	***p*-value**
Sample size	22	33	–
Week of gestation	33 (IQR 31.1–35.7)	31.7 (IQR 29.9–34)	N.S.
Week of labor	34.3 (IQR 32.4–36.1)	38.7 (IQR 38–40.1)	<0.001
Parity	0 (IQR 0–0.75)	0 (IQR 0–0)	N.S.
Maternal age (years)	32 (IQR 30–35.8)	32 (IQR 30–35)	N.S.

Abbreviation: N.S., no significant differences.

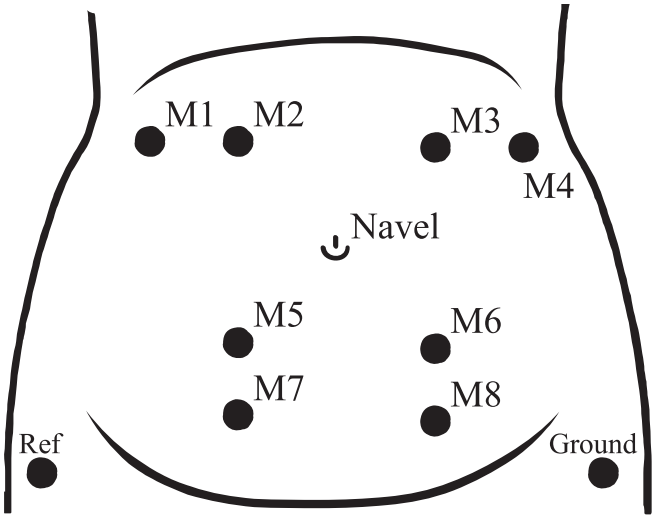

Fig. 1. The arrangement of the eight monopolar electrodes (M1–8) on the abdomen.

within seven days after hospitalization, and 40 % deliver at term [9]. Forty-four percent of these women have readmissions for preterm labor, thus leading to additional costs. Hence, the accurate prediction of imminent labor is crucial in TPL management. In this study, imminent labor is defined as deliveries within 7 days from the time of recording, in line with the practice established in the literature, since preterm labor can start 7 days before delivery [10–12]. Accurate identification of true preterm labor may prolong the pregnancy of real preterm infants with better and more personalized care [13], which may increase the survival rate in cases of extreme prematurity and reduce maternal and neonatal morbidity, while precise preterm labor prediction also reduces unnecessary hospitalization.

Early detection is key to preventing preterm delivery and minimizing its negative consequence. The most commonly used techniques in clinical practice are uterine dynamic monitoring by tocodynamometer and assessment of the cervical state (length, consistency and dilatation, effacement) and/or biochemical biomarkers such as fetal fibronectine and interleukin 6 [14,15]. These methods have achieved a limited degree of success (AUC ~ 67 %), with a high negative predictive value and low positive predictive value [15,16], i.e. none of these techniques can accurately predict the risk of prematurity.

Electrohysterography (EHG) has emerged as an alternative technique for precision uterine dynamic monitoring and predicting preterm labor, thanks to its high sensitivity. EHG is the recording of uterine myoelectrical activity on the maternal abdominal surface. EHG is made up of a slow wave (0.005–0.03 Hz) and a fast wave, which in turn is divided into fast wave low (0.1 to 0.34 Hz) and fast wave high (0.34 to 4 Hz) with its energy mainly distributed below 1 Hz and which has been associated with signal propagation and cell excitability, respectively [15,17–19]. Traditionally, the analysis of the EHG signal focused on characterizing the fast wave component by a set of temporal, spectral, and non-linear parameters [15,20,21] since the slow wave taken from surface recordings has a dubious physiological meaning due to overlapping with skin stretching and baseline fluctuation [19]. Previous studies have shown that signal amplitude increases as delivery approaches due to the major recruitment of uterine cells [19], while cell excitability also increases as pregnancy progresses, giving rise to the shifting of spectral content to a higher frequency [17,18]. Labor proximity is also related to higher signal predictability and regularity [18,20]. The latest studies sought to determine the propagation velocity and directionality of uterine contraction using multichannel EHG to identify new biomarkers for preventing preterm labor, with no agreement on the propagation direction [22–24].

Garfield et al. recently provided a new approach based on vectormyometriogram (VMG) to analyze EHG signals [19]. Similar to the well-known vectorcardiogram, which is a vector representation of the electrocardiogram, VMG is a spatio-temporal representation of uterine vector displacement based on the fact that the morphology of bioelectric waves depends on the geometric relationship between the magnitude of bioelectric events and the orientation of the electrodes [19]. Theoretically, uncorrelated disorganization of the bioelectric events shows a chaos vector map with major displacement divergence, while more organized events show a more coherent and smoother vector representation [19]. The vectorcardiogram has been shown to provide more information than the traditional electrocardiogram, with a higher sensitivity to detect myocardial infarction, ischemia, and hypertrophy [25–27]. VMG analysis may thus provide another potential indicator of the proximity of delivery for preterm labor prevention, which has not been considered previously in the literature. In a preliminary VMG study of both slow wave and fast wave components conducted on a few women in the active phase of term labor [19], Garfield et al. showed that the slow wave initiates fast wave activity clusters that activate muscle contractions, presenting a predominant up/down direction [19]. The percentage of slow wave downward-directed vectors increased from 58 % in EHG term recordings to 75 % in the 2nd stage of labor [19]. By contrast, the VMG of the fast wave component consists of multiple small amplitude loops without any specific direction in X–Y rather than a predominant direction, suggesting the dynamic behavior of the propagation direction [19]. However, there is no evidence in quantitative VMG analysis to predict imminent labor and/or preterm labor.

In the literature, the recurrence plot arose as an advanced non-linear method widely used to characterize dynamic vectorcardiogram behavior [28–30], since recurrence is a common feature of dynamic systems [31]. A recurrence plot is a graphical tool based on phase space reconstruction [32], which quantifies recurrences that occur in a displacement, where recurrence is the ability to return to the same state after a certain period [33], i.e. the trajectory returns to a previously visited area in the phase space. The recurrence plot can be used for visual and qualitative analysis of specific large- and small-scale patterns of dynamic systems. Recurrence quantification analysis (RQA) is the statistical quantification of a recurrence plot for the analysis of non-linear dynamic systems to assess laminar, divergent, or non-linear transition behavior by means of quantifying the diagonal and vertical lines of the recurrence plot [34]. RQA has been shown to be helpful in detecting phase transition even in short, non-stationarity and noisy data [32]. It has also been widely used to characterize biomedical signals [30,35,36] and to discriminate imminent labor and non-imminent labor in women with TPL [37].

The aim of this work was thus to determine the feasibility of detecting imminent/non-imminent and preterm/term labor in women with TPL using RQA of VMG and to compare their discriminatory capacity with temporal, spectral and non-linear parameters derived from

Table 2
Summary of Corrupted Segments, Mean Duration, and Associated Rejection Rate per Record. Presented as Median (Interquartile Range, Q1–Q3).

VMG	Number of corrupted segments per record	Average duration (seconds) per record	Rejection rate per record
X1-Y1	1 (IQR 0–2)	83 (IQR 0–288)	8.83 % (IQR 2.08–28.06 %)
X1-Y2	1 (IQR 0–2)	81.67 (IQR 0–288)	10.29 % (IQR 2.36–30.24 %)
X2-Y1	1 (IQR 0–2)	71.33 (IQR 0–287)	7.5 % (IQR 1.86–24.22 %)
X2-Y2	1 (IQR 0–2)	78.17 (IQR 0–310.38)	11.04 % (IQR 2.15–26.68 %)

bipolar EHG. We also wanted to assess the relationship between VMG recurrence statistics and both gestational age and time to delivery.

2. Materials and methods

2.1. Database

We used a total of 55 EHG records from singleton pregnant women with threatened preterm labor (TPL) between the 26th and 36th week of gestation recruited at the Department of Gynecology and Obstetrics, Peking Union Medical College Hospital, Beijing [38]. The patients were followed up until delivery and provided the following clinical data: week of gestation, week of labor, maternal age and parity. We further divided the entire database into preterm labor and term labor groups according to the gestational age at the time of delivery. We also analyzed the ability of EHG to detect imminent labor (delivery in less than 7 days) in women with TPL. Table 1 gives the demographic description of the dataset. The study adhered to the guidelines of the Declaration of Helsinki and was approved by the Institutional Review Board of the hospital (Register Number 2018/0530). The patients were informed of the nature of the study and gave their written informed consent.

We conducted a 30-min simultaneous recording of multichannel EHG and tocographic signals on each patient, as shown in Fig. 1. Physiologically, closely spaced bipolar recordings are mainly sensitive to local bioelectrical activity close to the surface between the electrode, while distant electrodes can pick up the propagation events from the entire uterus [19]. We strategically positioned eight electrodes on the maternal abdomen, covering practically the whole uterus and collected the information in both horizontal and vertical directions to obtain a 2D VMG. Electrodes 1 to 4 were placed on the fundus, electrodes 5 and 6 were symmetrically placed below the navel, 7 and 8 were placed on the pubic symphysis and the reference and ground electrodes were placed on each side of the iliac crests. The technical description of the device used was: bandwidth of the EHG channels is 0–70 Hz, gain of amplifiers is 24, sampling rate is 250 Hz. The device included an ADS1299 analog-to-digital converter (ADC), a 24-bit delta-sigma ADC.

The EHG signals were further band-pass filtered between 0.1 and 1 Hz using a fifth-order digital zero-phase Butterworth filter, since EHG distributes its spectral content within this bandwidth [15]. We conducted the analysis using three specific bandwidths: the whole bandwidth (0.1–1 Hz), fast wave low (FWL, 0.1–34 Hz), and fast wave high (FWH, 0.34–1 Hz) [18,19,39]. The bandwidth selection is a trade-off between computational cost and the accurate representation of the recurrence plot. In this regard, the recurrence plot is based on thresholding the distance between 2-dimensional points to determine whether or not they are recurrent (as explained below), using information from 0.1 to 1 Hz is quite an accurate estimation of uterine vectors without loss of generalities. In addition, EHG signals were downsampled to 4 Hz.

2.2. Recurrence quantification analysis of vectormyometriogram

Taking into account the fact that the inter-electrode distance of bipolar recordings should be as long as possible and similar in the X-Y

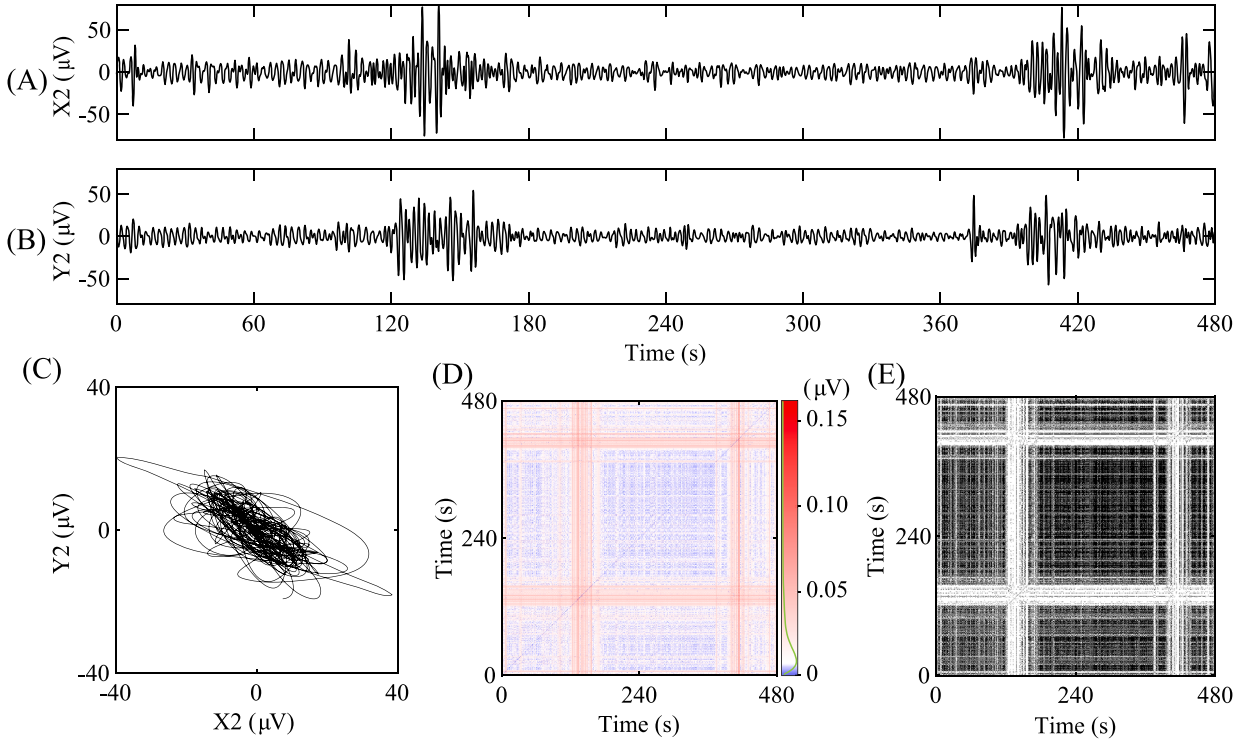

Fig. 2. Recurrence plot of VMG from a woman with TPL at 36 weeks of gestation who finally delivered prematurely. Only 480 s of signal were represented to simplify the visualization, instead of the complete record. (A) Horizontal bipolar EHG X2 (B) Vertical bipolar EHG Y2. (c) 2D-VMG. (D) Recurrence matrix, in which the distance between phase space states is coded by color. Red indicates high distant phase space states. (E) Recurrence plot after thresholding with its median value, where black pixels represent recurrence points.

direction to be analogous to that used by Garfield et al. [4], we obtained two horizontal (X1 = M1 – M3 and X2 = M2 – M4) and two vertical components (Y1 = M2 – M7 and Y2 = M3 – M8) in orthonormal X, Y directions. We then formed four 2-D VMG configurations (X1-Y1, X1-Y2, X2-Y1, and X2-Y2). Each monopolar channel (M1–M8) in the EHG records were later reviewed by two experts in a double-blind process to discard all the corrupt signal segments (motion artifacts and respiration interference, among others) [3]. Subsequently, a common segmentation was obtained from the monopolar channels of each 2-D VMG configuration. Table 2 summarizes the commonly used statistical measures of the corrupted segments with their mean duration and rejection rate.

Our aim was to study the robustness of recurrence quantitative analysis against motion artifacts and carried out the same signal processing pipeline for both raw data and motion artifact-free data, which consisted of discarding the corrupted segments and joining together the remaining physiological activities to construct a single recurrence plot for each EHG record [41–48] due to the fact that longer time series are preferred for a more robust recurrence quantification analysis [49]. A shorter time series may not adequately represent the complete recurrent behavior of the signal [32]. As detailed in Appendix A, we compared the ability of the different VMG configurations to detect preterm and imminent labor in women with TPL by assessing the feature number with statistically significant differences between the groups and intergroup separability by calculating the Cohen's effect size and found X2-Y2 the best configuration to detect preterm and imminent labor in women with TPL. We only focus on X2-Y2 in the following sections of the paper for the sake of clarity and brevity.

We carried out a RQA analysis of uterine VMG. Considering the $\vec{v}(i)$ 2-dimensional phase space represented by the i-th point of time series X and Y, we first computed the recurrence matrix of dimension N x N, which contains the distances of each point $\vec{v}(i)$ from all the other $\vec{v}(j)$ in the phase space [31], where N is the total sample number of the time series. We then considered the recurrence point as the one that satisfies that $\vec{v}(j)$ was close enough to $\vec{v}(i)$ with a distance less than a predefined threshold ε, thus obtaining the recurrence plot:

$$RP(i,j) = \Theta(\varepsilon - \|\vec{v}(j) - \vec{v}(i)\|)$$

where $\|\|\cdot\|\|$ the Euclidean distance norm and Θ is the Heaviside function [32]. Fig. 2 shows an example of both X2 (trace A) and Y2 (trace B) time series, its corresponding 2D-VMG (trace C), recurrence matrix (trace D), and thresholded recurrence plot (trace E) obtained from a woman with TPL who finally delivered prematurely.

As mentioned above, the recurrence plot is a graphical representation for qualitative analysis. In this work, we used RQA, which quantifies the recurrence of the dynamic system and provides a set of scalar metrics from the recurrence plot [32]. RQA is based on identifying continuous sequences of recurrence points, which form vertical, horizontal or diagonal lines and how frequently they are repeated in the whole recurrence plot. Consecutive recurrence points imply similar structures along the original time series. Thus, diagonal lines represent segments with synchronous periodicity, while vertical or horizontal, i.e., laminar structures, reflect high stability signals [32]. We used four typical RQA metrics to quantify the periodicity, complexity, and stability of the recurrence plot of VMG: determinism, longest diagonal (L_{max}), entropy and laminarity. As pregnancy progresses, the rising synchronization and rhythm involve increased periodicity and predictability [18,20].

• Determinism: characterizes diagonal lines parallel to the diagonals of an iterated graph. The maximum determinism coefficient values exist in periodic systems, in which the disappearance of periodicity causes the fragmentation of oblique lines [32].

$$DET = \frac{\sum_{l=l_{min}}^{N} l\,P(l)}{\sum_{l=1}^{N} l\,P(l)} \tag{2}$$

where P(l) is the histogram of diagonal lines, l is the diagonal line length, l_{min} is the minimal length of a diagonal line and N is the length of the time series.

• L_{max}: is the length of the longest diagonal and is a measure of the stationarity of the signal. The diagonal length of a given signal indicates the duration of the periodic component, so that the L_{max} value is generally higher for systems with regular dynamics, i.e. stationary systems, while the L_{max} value is lower for systems with irregular behavior [32].

$$L_{max} = \max\left(\{l_i\}_{i=1}^{N_l}\right) \tag{3}$$

where N_l is the total number of diagonal lines.

• Shannon entropy: estimates the variability in the distribution of diagonals [32]. Classical entropy measures generally increase their magnitude when the signal complexity and chaos rise. However, the entropy obtained from a recurrence plot correlates with the inverse of the largest Lyapunov exponent and therefore has an entirely opposite meaning, decreasing when signal complexity and chaos increase [31,50].

$$ENTR = -\sum_{l=l_{min}}^{N} p(l)\ln(p(l)) \tag{4}$$

where p(l) = is the probability of finding a line of exact length l.

• Laminarity: characterizes the vertical lines on the graph and is a measure of signal stability. It describes the percentage of points belonging to the vertical lines against the total rate of recurrence points [32].

$$LAM = \frac{\sum_{w=w_{min}}^{N} wP(w)}{\sum_{w=1}^{N} P(w)} \tag{5}$$

where P(w) is the histogram of vertical lines, w is the length of verticals, w_{min} is the minimal length of a diagonal line.

As pregnancy progresses, the rising synchronization and rhythm involve increased periodicity and complexity [18,20]. Indeed, determinism, L_{max} and entropy, which characterize the periodicity and complexity properties of the signals, are expected to increase as labor approaches. Likewise, the increase in signal stability as delivery nears is reflected in increased laminarity.

For each scenario (imminent or preterm labor) and each analysis bandwidth, we conducted a grid search of both threshold ε and minimum length of both diagonal and vertical lines ($l_{min} = w_{min}$) to maximize the separability between the groups using the Wilcoxon Rank-Sum Test (α = 0.05). The hyperparameter was optimized by sweeping the threshold ε from 0.5 to 1.5, with a step of 0.1 [35,49,51] times the median phase distance and the minimum number of recurrence points from 2 to 10 [32,52].

2.3. Statistical analysis

Due to the intrinsic relationship between the labor trigger with gestational age, we subdivided the database into 4 subgroups by gestational age to visually analyze the data: W1 (26–30 weeks), W2 (31–32 weeks), W3 (33–35 weeks), and W4 (36–37 weeks), and subdivided the database into 4 subgroups according to time to delivery: T1 (less than 24 h), T2 (more than 24 h but less than 1 week), T3 (1–2 weeks), and T4 (3 or more weeks). Spearman's rank correlation (α = 0.05) was used to determine whether the recurrence statistics had a significant relationship with gestational age (W1–W4) and time to delivery (T1–T4), using all the available data. We also determined the ability of the recurrence statistics obtained from the VMG to detect both imminent and preterm labor in women with TPL for both the whole bandwidth (WBW, 0.1–1 Hz), FWL and FWH. We used the Wilcoxon rank sum test (α = 0.05) and also computed Cohen's effect size to determine the magnitude effect. The *p*-value indicates the existence of

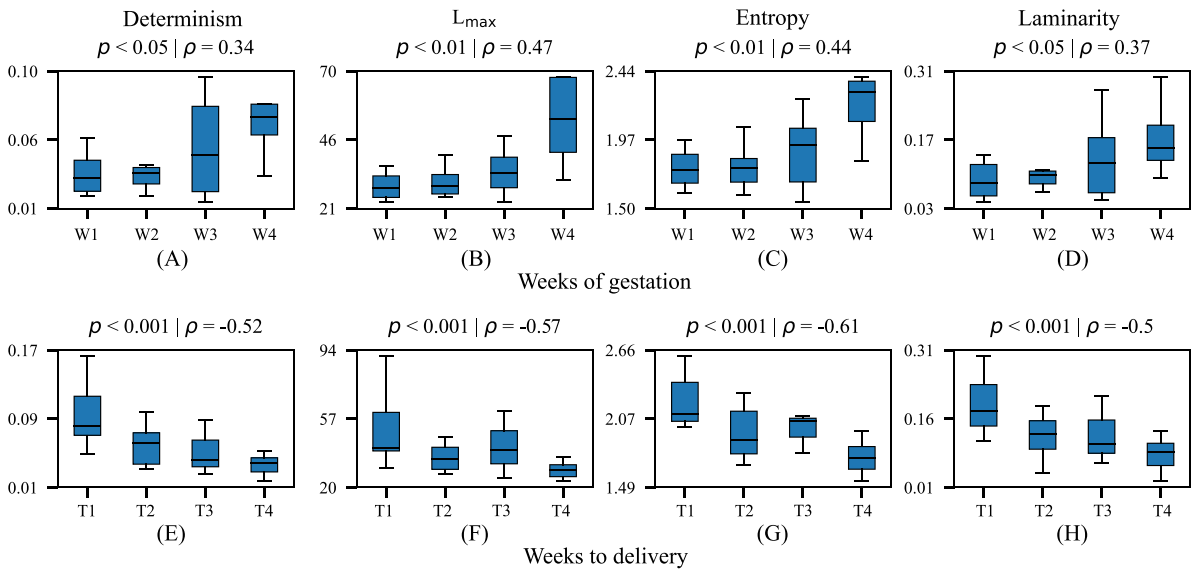

Fig. 3. Box and whiskers plot of recurrence metrics (determinism, maximum diagonal length, Shannon entropy, and laminarity) computed in FWH bandwidth as a function of the week of gestation (upper row) and time to delivery (lower row). The P-value (p) < 0.05 shows that recurrence statistics are significantly linked with gestational age and time to delivery. ρ is Spearman's Rank Correlation Coefficient. The data is organized into distinct categories: gestational age subgroups categorized as W1 (26–30 weeks), W2 (31–32 weeks), W3 (33–35 weeks), and W4 (36–37 weeks), and time to delivery subgroups categorized as T1 (less than 24 h), T2 (more than 24 h but less than 1 week), T3 (1–2 weeks), and T4 (3 or more weeks).

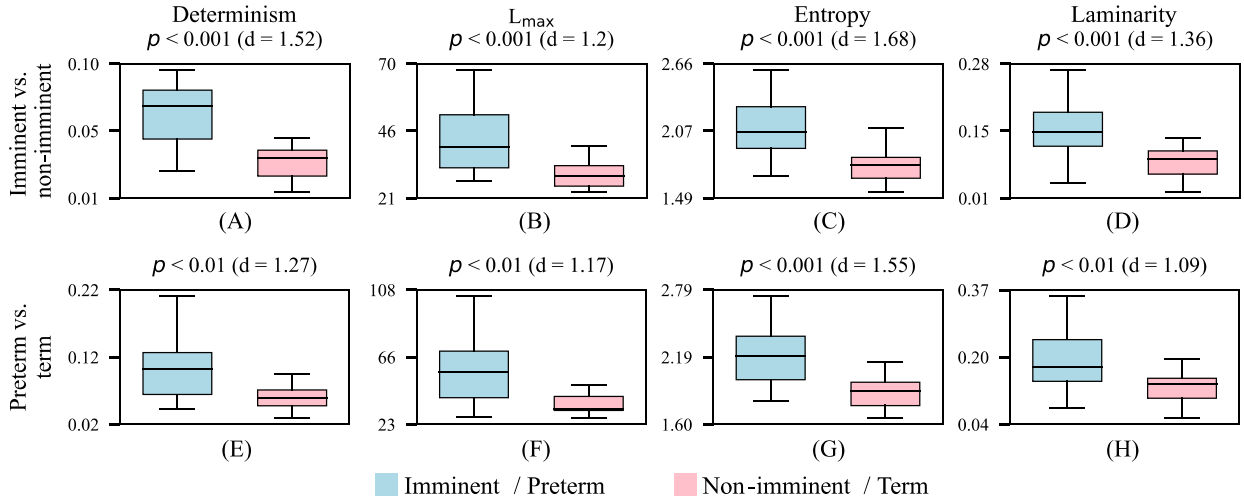

Fig. 4. Box and whisker plots of recurrence metrics of imminent vs. non-imminent (threshold = 0.8 and minimum number of points = 8) and preterm vs. term (threshold = 0.9 and minimum number of points = 8) groups of women with TPL. The configuration of the EHG-vector is X2-Y2 and in the FWH bandwidth. p is the p-value of Wilcoxon Rank-Sum Test, and "d" is the Cohen's effect size. Blue boxes are for the imminent/preterm group, and red boxes are for the non-imminent/term group.

the effect, the Cohen' effect size gives us its magnitude and its sign reflects the direction of the effect, while its sign indicates the nature of the effect. A negative effect size suggests a lower average value in the imminent/preterm group than in the non-imminent/term group, whereas a positive effect size denotes the opposite [53]. To determine the robustness of RQA against motion artifacts, we also compared their performance between raw data and motion artifact-free data identified by experts in a double-blind process.

2.4. Comparison with bipolar EHG parameters

Finally, we compared the discriminatory capability between groups (preterm vs. term, imminent vs. non-imminent) of the recurrence statistics from VMG with classical bipolar EHG parameters. We used four commonly used EHG parameters that have been proven to provide relevant labor prediction. For both the X2 and Y2 bipolar channels, we computed the peak-to-peak amplitude, related to cell recruitment, the dominant and median frequency used to assess uterine cell excitability, the sample entropy to quantify signal regularity, and time reversibility to assess the non-linear degree of the signal with greater time reversibility, indicating more stability [15,18,20,21,54]. Peak-to-peak amplitude, sample entropy and time reversibility were calculated in the 0.34–1 Hz range (we did not obtain better results for 0.34–4 Hz), while the dominant median frequency was computed in the 0.2–1 Hz bandwidth, in which the EHG power spectra is predominantly distributed [18,20,21]. The characterization was performed using a sliding window of 120 s with a 50 % overlap [55]. Each patient was then taken as a representative value for each parameter of the median value of the windows. The Wilcoxon Rank-Sum Test was again used to determine the statistical difference between the groups and the Cohen's effect size was

Table 3
P-values (effect size) for of recurrence metrics of imminent/preterm versus. non-imminent/term groups of women with TPL. The configuration of the EHG-vector is X2-Y2. Very large effect sizes > 1.2 are highlighted in bold.

Bandwidth	Metric	Imminent vs. non-imminent		Preterm vs. term		Σ *p*-values
		Raw data	Motion artifact-free data	Raw data	Motion artifact-free data	
WBW	Determinism	<0.05 (0.64)	<0.01 (1.12)	<0.01 (0.9)	<0.05 (0.88)	$\Sigma(p < 0.05) = 14$
	L_{max}	<0.01 (0.78)	<0.01 (0.69)	<0.05 (0.61)	<0.01 (1.02)	$\Sigma(p < 0.01) = 7$
	Entropy	<0.05 (0.9)	<0.01 (1.17)	<0.01 (1)	<0.05 (1)	$\Sigma(p < 0.001) = 0$
	Laminarity	N.S. (0.57)	<0.05 (0.87)	<0.05 (0.81)	N.S. (0.77)	
FWL	Determinism	N.S. (0.44)	<0.05 (0.9)	<0.05 (0.77)	<0.05 (0.64)	$\Sigma(p < 0.05) = 9$
	L_{max}	N.S. (0.39)	<0.05 (0.55)	N.S. (0.62)	<0.01 (0.75)	$\Sigma(p < 0.01) = 1$
	Entropy	<0.05 (0.72)	<0.05 (0.96)	<0.05 (0.74)	<0.05 (0.75)	$\Sigma(p < 0.001) = 0$
	Laminarity	N.S. (0.42)	N.S. (0.64)	N.S. (0.71)	N.S. (0.6)	
FWH	Determinism	<0.01 (0.93)	**<0.001 (1.52)**	**<0.001 (1.3)**	**<0.01 (1.27)**	$\Sigma(p < 0.05) = 16$
	L_{max}	<0.001 (0.78)	**<0.001 (1.2)**	**<0.01 (1.23)**	<0.01 (1.17)	$\Sigma(p < 0.01) = 16$
	Entropy	<0.001 (1.16)	**<0.001 (1.68)**	**<0.001 (1.48)**	**<0.001 (1.55)**	$\Sigma(p < 0.001) = 10$
	Laminarity	<0.01 (0.92)	**<0.001 (1.36)**	**<0.001 (1.27)**	<0.01 (1.09)	
Σ *p*-values by column	$\Sigma(p < 0.05)$	8	11	10	10	
	$\Sigma(p < 0.01)$	5	7	6	6	
	$\Sigma(p < 0.001)$	2	4	3	1	

Abbreviation: N.S., no significant differences.

Table 4
P-values (effect size) for of EHG parameters of imminent/preterm versus. non-imminent/term groups of women with TPL.

Channel	Clinical scenario	Peak-to-peak amplitude	Dominant frequency	Median frequency	Sample Entropy	Time reversibility
X2	Imminent vs. non-imminent	N.S. (0.56)	N.S. (0.35)	N.S. (-0.04)	N.S. (−0.71)	N.S. (0.57)
	Preterm vs. Term	N.S. (0.64)	N.S. (0.11)	N.S. (0.01)	<0.01 (−1)	N.S. (0.42)
Y2	Imminent vs. non-imminent	N.S. (0.84)	N.S. (0.11)	N.S. (-0.47)	<0.01 (−1.21)	N.S. (0.41)
	Preterm vs. Term	N.S. (0.59)	N.S. (−0.51)	N.S. (-0.32)	<0.01 (−1.25)	<0.05 (0.66)

Abbreviation: N.S., no significant differences.

Table A1
Number of statistically significant differences (Wilcoxon Rank-Sum Test) for each X-Y VMG configuration, considering both the imminent vs. non-imminent and preterm vs. term approaches, using both raw and motion artifact-free data.

	Imminent vs. non-imminent								Preterm vs. term								
	Raw data				Motion artifact-free data				Raw data				Motion artifact-free data				
	WBW	FWL	FWH		WBW	FWL	FWH		WBW	FWL	FWH		WBW	FWL	FWH		$\Sigma(p < 0.05)$
X1-Y1	3	1	4	**8**	4	3	4	**11**	4	2	4	**10**	4	1	4	**9**	**38**
X1-Y2	2	0	4	**6**	4	0	4	**8**	4	1	4	**9**	4	1	4	**9**	**32**
X2-Y1	2	0	3	**5**	3	0	4	**7**	1	0	4	**5**	1	0	2	**3**	**20**
X2-Y2	3	1	4	**8**	4	3	4	**11**	4	2	4	**10**	3	3	4	**10**	**39**
$\Sigma(p < 0.05)$	10	2	15	27	15	6	16	37	13	5	16	34	12	5	14	31	

computed to determine the magnitude effect.

3. Results

Fig. 3 shows the changes in the recurrence metrics computed in the FWH bandwidth throughout the third trimester of pregnancy (upper row) and time to delivery (lower row). The four recurrence statistics showed an upward trend as labor progresses, with subtle changes between the subgroups W1, W2 and W3. By contrast, the subgroup W4 showed an abrupt increase for the four recurrence statistics (see Fig. 3 (A)–(D)). The four recurrence statistics considerably increased from early (W1) to late (W4) stages: determinism (0.035 ± 0.011 vs. 0.077 ± 0.041), L_{max} (28.8 ± 4.5 vs. 52.2 ± 16.4), entropy (1.768 ± 0.116 vs. 2.197 ± 0.24), and laminarity (0.086 ± 0.034 vs. 0.173 ± 0.078). We found that the relationship with gestational age is generally moderate and statistically significant, with correlation coefficients ranging from 0.34 and 0.47 for determinism and L_{max}, respectively. The recurrence statistics obtained higher correlation coefficients than gestational age with time to delivery (see Fig. 3(E)–(H)), ranging from −0.50 to −0.61 for laminarity and Shannon entropy respectively. The other bandwidths analyzed showed similar trends with weaker correlation coefficients (results not shown).

Fig. 4 shows examples of box and whisker plots of the recurrence statistics to distinguish women with TPL who finally deliver imminently/prematurely, or not, for FWH bandwidth and motion artifact-free data. Specifically, the imminent/preterm labor group provided higher recurrence statistics than the non-imminent/term labor group, as it did for the FWL, the whole bandwidth and for raw data. Regardless of the recurrence statistics, the distribution of the imminent/preterm group is shifted upward with respect to that of the non-imminent/term class. The four imminent and preterm labor recurrence statistics of were significantly higher than non-imminent and term labor, with a large effect size (d > 1) in all cases. The proposed method better differentiated imminent vs. non-imminent labor (*p*-value < 0.001 and the very large effect sizes > 1.2) than preterm vs. term labor. Shannon entropy outperformed determinism (*p*-values < 0.001 and effect sizes of 1.68 and 1.58 to detect imminent and preterm labor, respectively), while this latter in turn performed better than L_{max} and laminarity for both clinical scenarios.

Table 3 shows the results of the recurrence metrics for different imminent vs. non-imminent and preterm vs. term labor groups in women with TPL for WBW, FWL and FWH bandwidths, and for raw data and motion artifact-free data. As for the bandwidth analysis, FWL

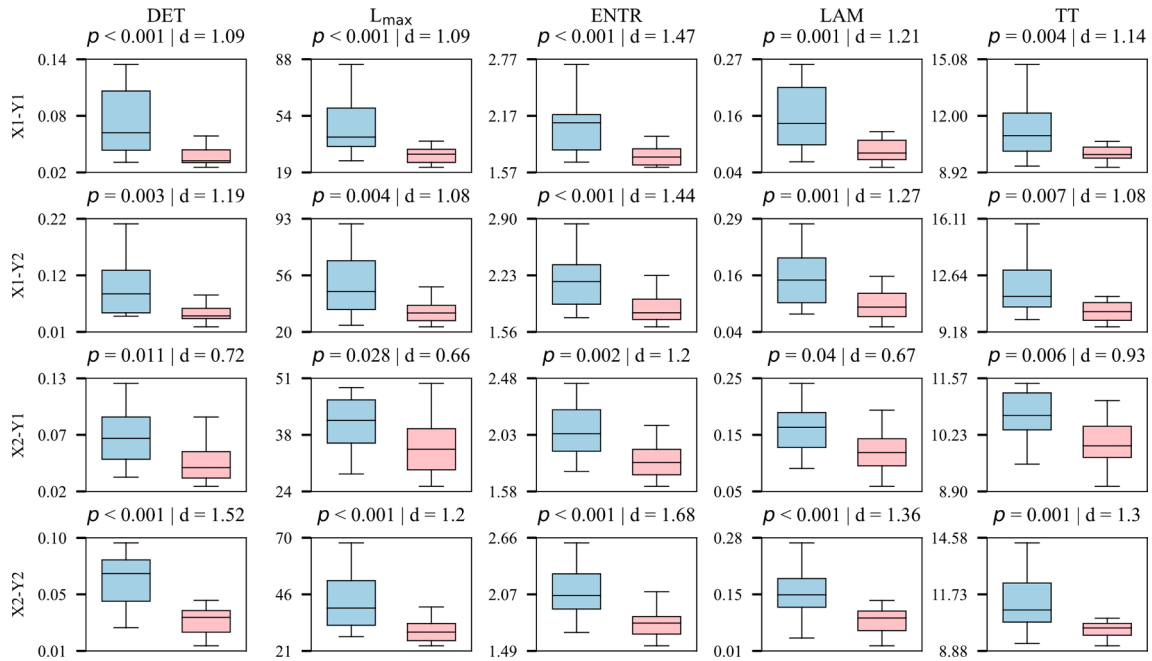

Fig. A1. Box and whisker plot representing recurrence statistics for the imminent vs. non-imminent approach in the FWH bandwidth using motion artifact-free data. The p-value of the Wilcoxon Rank-Sum Test is denoted as 'p', and the Cohen's effect size is represented as 'd'. The blue boxes represent the imminent group, while the red boxes represent the non-imminent group.

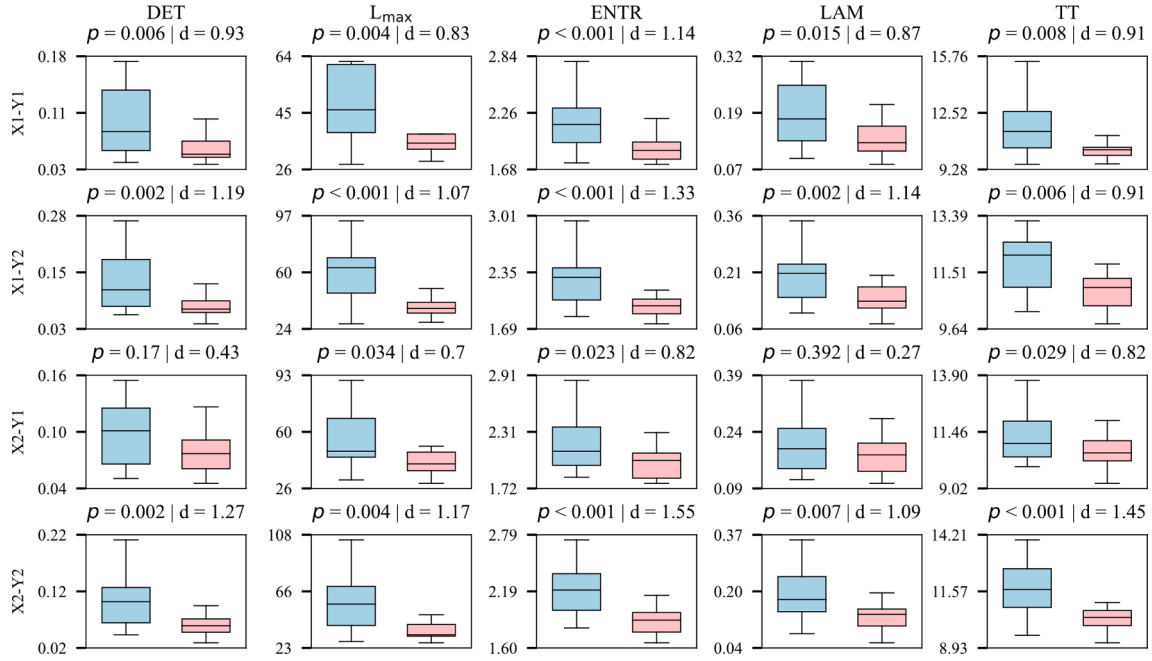

Fig. A2. Box and whisker plot representing recurrence statistics for the preterm vs. term approach in the FWH bandwidth and using motion artifact-free data. The p-value from the Wilcoxon Rank-Sum Test is denoted as 'p', and the Cohen's effect size is represented as 'd'. The blue boxes represent the preterm group, while the red boxes represent the term group.

performed worst, with the lowest number of statistically significant differences between groups. Although the WBW and FWH bandwidths presented a similar number of p-values < 0.05, the FWH bandwidth performed better with a higher number of p-values < 0.001 and very large effect sizes ($d > 1.2$). Regarding the robustness of the method against motion artifacts, artifact-free data performed better than raw data to differentiate imminent vs. non-imminent labor (more significant difference with a larger effect size). Even so, raw data preserved the ability to detect imminent labor, especially for the FWH bandwidth. Both raw and motion artifact-free data showed a similar ability to discriminate preterm and term labor, although raw data seems to obtain larger effect size.

For the recurrence statistics, Shannon entropy and determinism obtained similar results and outperformed L_{max} and laminarity. Regardless of bandwidth, clinical scenario and input data, Shannon entropy and determinism obtained statistically significant differences between the groups, with 12 and 11 significant p-values out of a possible 12, respectively. Laminarity seemed to be highly sensitive to the bandwidth,

obtaining promising results for the FWH bandwidth.

Table 4 shows the discriminatory capability of temporal, spectral and non-linear parameters of motion artifact-free bipolar channels X2 and Y2 in the FWH bandwidth. Peak-to-peak amplitude, dominant frequency and median frequency did not show any significant differences between the groups. For both X2 and Y2, preterm group exhibited significantly lower sample entropy than the term group (p-value < 0.01, effect size < -1). By contrast, only Y2 yielded significant differences in discriminating imminent and non-imminent labor (p-value < 0.01, effect size $= -1.21$). For time reversibility, preterm labor only presented significantly higher values than the term group for Y2 (p-value < 0.05, effect size $= 0.66$).

4. Discussion

4.1. Physiological interpretation of VMG changes during pregnancy

This study aimed to determine the ability of recurrence statistics obtained from the VMG to detect imminent or preterm labor in women with TPL, which mainly describe VMG properties of periodicity (determinism and L_{max}), complexity (Shannon entropy) and stability (laminarity), which evolves during pregnancy [18,56–58]. We found both determinism and L_{max} increase, which quantify in diagonal lines as pregnancy advances and as labor approaches, suggesting an increase in the periodicity of uterine vector displacement [32]. Delivery proximity also is linked to an increase in signal stability [41,54,59], as reflected in the laminarity. RQA's Shannon entropy correlates with the inverse of the maximum Lyapunov exponent, which indicates chaotic behavior [31,50]. Shannon entropy increase associated with pregnancy progression can be interpreted as decreased chaos degree [60,61], i.e labor proximity is linked to increased organization and higher signal predictability of the uterine vector displacement [18,54,62]. These findings are attributed to electrophysiological changes in the uterus during pregnancy [18,54,62]. Garfield hypothesized that, in the early stages of gestation, there is a higher number of small "patches or clusters" of local electrical activity dispersed in the uterus, resulting in scarce and uncoordinated electrical activity [19]. As labor progresses, the gap junctions form and enhance the propagation of electrical activity, which may reduce the number of "patches or clusters" and increase the patch areas [19]. As a result, in advanced pregnancy electrical activity becomes intense and synchronized/coordinated and no longer reflects the local uterine activity of the "patches or clusters", reaching a maximum during labor. Uterine contractions also increase as labor approaches [56,57], giving rise to a rhythmic uterine electrical activity (3 contractions in 10 min) during the first stage of the active phase of labor. It has been shown that signal periodicity and predictability both increase as do synchronization and rhythm [18,20]. Synchrony between a pair of channels is defined as the tendency to maintain a nearly constant phase difference over a period of time, although the analyzed phase of each channel may vary considerably during this period [58,63]. In the present work, we found an abrupt increase in recurrence statistics in women who were close to delivery, and mainly at gestational ages ranging from 35 to 37 weeks, which may derive from the increased synchronization during this time interval. Indeed, studies in the literature point out that the gap junction formations abruptly increase few days before delivery and reach a maximum during labor [19].

Our results disagree with those of Borowska et al., who used a single EHG channel to reconstruct phase space by optimizing both the embedding dimension and time delay in the sliding window and computed recurrence statistics to detect labor imminence in 20 women with TPL between the 24th and 28th weeks of gestation. They found that the women close to labor showed significantly lower values for recurrence rate, determinism, Shannon entropy and laminarity than non-imminent women (p-value < 0.001) [37]. We believe that this difference in the recurrence statistics changes throughout pregnancy may be partially due to the bias of small database [64]. In the present work, we reconstructed the phase space from 2D-VMG using the embedding dimension $m = 1$ and time delay $\tau = 1$, which considerably simplifies the data processing pipeline and allows the recurrence statistics to be estimated from the whole record rather than the sliding window. Longer time series are preferred for a more robust recurrence quantification analysis [49], as a shorter time series may not adequately represent the signal's complete recurrent behavior [32]. Our results are in line with those found by Di Marco et al. that recurrence statistics from 3 bipolar EHG showed higher periodicity and lower complexity as labor approaches. Their findings revealed that the recurrence statistics assessed for a single horizontal EHG, determinism (p-value < 0.05), Shannon entropy (p-value < 0.005), and Lmax (p-value < 0.05) could effectively differentiate preterm delivery in women undergoing regular check-ups, which were poorer indicators than sample entropy (p-value < 0.005) [52]. By contrast, our results showed that VMG recurrence statistics achieved a better discriminatory capacity to detect imminent and preterm labor in women with TPL (p-value < 0.001), outperforming sample entropy. Although a direct comparison is not feasible due to the differences in the databases and the clinical scenario, we speculate that VMG is more sensitive in detecting imminent/preterm labor than conventional bipolar EHG because VMG assesses the variation of the instantaneous uterine vector displacement viewed from a longer distance associated with propagated events rather than local activity [19,65].

4.2. EHG biomarkers to detect preterm and imminent labor: classical bipolar EHG vs. VMG recurrence statistics

As for the preterm labor detection, many studies in the literature have focused on developing a prediction system based on EHG in women with regular check-ups (physiological recording without any drug effects), obtaining promising results [15,66], while there are fewer studies conducted on women with TPL [15,66]. Even so, there is increasing evidence on the feasibility of detecting imminent labor in women with TPL by the EHG [10,11,55,67]. In this work, we dealt with and compared the performance of the recurrence statistics obtained from the uterine vector displacement in different bandwidths to detect both imminent and preterm labor in women with TPL. Recurrence statistics computed from the FWH bandwidth outperformed those of the WBW and this, in turn, performed better than FWL, which was in line with findings in previous works [18,20,54]. Non-linear parameters computed in the FWH bandwidth offered better separability between the term and preterm group in women with regular check-ups [20,68]. Non-linear parameters also showed consistent tendencies for different obstetric scenarios (antepartum, during labor and postpartum) when computed in the FWH bandwidth but not in the whole bandwidth [54]. This may be associated with the FWH components that mainly appear close to delivery and are hallmark characteristics of the proximity of delivery [18,20,68].

We also compared VMG recurrence statistics with the classical temporal, spectral and non-linear parameters from bipolar channels to identify the imminence and preterm labor risk. In the present work, the peak-to-peak amplitude dominant frequency and median frequency were unable to differentiate between imminent and non-imminent or preterm and term labor (no significant differences between the groups). This result was consistent with our previous results in studies that attempted to discriminate between imminent vs. non-imminent labor using EHG parameters from women with TPL taken from another database [10,55]. We believe that the lack of sensitivity may be associated with the specific TPL clinical scenario and the fact that the EHG recordings were carried out in different phases of tocolytic treatment with the aim of inhibiting uterine contractions to block oxytocin receptors by reducing cell excitability [69,70]. In fact, in a previous study we found that TPL women who delivered preterm presented a time delay in the reduction of high-frequency EHG components in comparison to TPL women who delivered at term, which is probably due to the presence of a higher number of oxytocin receptors expressed by the

myometrial cells in the former [71]. By contrast, sample entropy, a widely used parameter to quantify signal regularity and predictability [15,18,21,66], was the most sensitive, even more so than time reversibility [54], to detect imminent and preterm labor in women with TPL. Our results also suggest that VMG recurrence statistics outperformed classical EHG parameters, and provided reliable indicators of imminent labor in TPL women that will allow clinicians to design a patient-oriented strategy of prolonging pregnancy, as long as possible to enhance perinatal surveillance and reduce unnecessary hospitalizations for non-imminent labor women. In comparison to non-imminent labor group, imminent labor group presented significant higher gestational age which may partially explain the higher recurrence statistics and lower sample entropy. However, considering the subtle electrophysiological changes throughout pregnancy that abruptly increase close to delivery, we believe this difference is mainly due to labor imminence rather than gestational age. Also, compared to sample entropy, VMG recurrence statistics provided more significant information for identifying the preterm labor risk in TPL women, thus constituting biomarkers able to detect the underlying mechanism that triggers labor for better preventing preterm labor.

4.3. Limitations and future directions

Despite the promising results, this study is not exempt from limitations. Firstly, the actual database of TPL women was relatively small, so that detecting imminent/preterm labor was especially challenging. A small number of samples tends to bias the statistical test, since the sample is not representative of all the pregnancy cases [72]. Future work with a larger database is therefore still needed to further corroborate the clinical usefulness of the proposed method for preventing preterm labor in TPL women, as well as regular check-ups. RQA from the VMG outperformed classical temporal, spectral and non-linear parameters to predict imminent and preterm labor in TPL women, although we did not analyze the mutual and complementary information among them to design a robust and generalizable system for preventing preterm labor based on EHG [21,68].

On the other hand, motion artifacts remain a challenge for the scientific-technical community, constituting the main barrier to transferring the EHG technique to clinical practice. Robust data processing against motion artifacts is thus of great interest to extract the reliable biomarkers embedded in the EHG and promote the transfer of EHG to clinical practice. Motion artifacts, which usually present an abrupt change of signal amplitude, not only distort the spectral content distribution, but may also alter the threshold to obtain the recurrent points, and consequently the diagonal and vertical lines. The recurrence statistics estimated from raw data may thus greatly differ from their true value. The problem relies on the fact that motion artifacts have a widely varied morphologies, i.e. they can alter in different way for each EHG record [40]. This may explain the fact that raw data slightly outperform motion artifact-free data to detect preterm labor. By contrast the performance of raw data was much less effective than motion artifact-free data to differentiate the imminent and non-imminent labor groups, while the removal of corrupted segments may cause a slight variation of the diagonal and /or vertical line (depending on the duration of the corrupt segments) giving rise to bias in the recurrence statistics. In this work, we compared raw and motion artifact-free data to assess their ability to detect imminent and preterm labor and found that the RQA of VMG preserve the discriminatory capability to differentiate imminent/preterm and non-imminent/term labor (p-value < 0.05), although generally with a lower Cohen's effect size, suggesting that the proposed method is robust to a certain extent against motion artifacts. Thiel et al. showed that the same determinism values were achieved by adequately setting the threshold for a clean signal and for the same contaminated signal with 10 % Gaussian noise [73]. It has also been reported that as the noise level increases, the recurrence metrics value decreases slightly, when the noise level becomes very high, the recurrence metrics values of all the signals suddenly changed [74]. For physiological signals, Webber et al. claim that recurrence plots are robust against non-uniformity, dynamic noise, system transitions and state changes, which are very frequent in standard physiological systems [75]. However, motion artifacts, which present a very varied morphology, are much more complex than synthetized noise [40]. Future works designed to determine the robustness of recurrence statistics against motion artifacts are still needed to corroborate this hypothesis. In this work, we discarded motion artifacts, which typically distort the spectral content distribution, from EHG recordings by experts [39,40]. Although manual segmentation by experts provides the most reliable results, it is a laborious process. Many efforts have focused on the automatic detection of uterine contractions in EHG [38,40,76], but its application in the early stage with a lower signal-to-noise ratio is still unclear.

Also, preterm labor is not exclusively associated with uterine dynamics measured by EHG, but also with other multiple physiological mechanisms. In the literature, cervix measurement and chemical biomarkers, such as cervical length, fetal fibronectin, and interleukin 6, have been established as valuable predictors of preterm birth [15,18,62]. Incorporating these clinical data into preterm birth prediction models [10] could still improve their overall performance, although further studies are still needed to corroborate this hypothesis. Despite these limitations, we believe that this is the first study to provide reliable evidence of the feasibility of using the VMG to prevent preterm labor in women with TPL.

5. Conclusions

In this work we not only confirmed the existence of a recurrence pattern of uterine vector displacement but also determined their changes throughout pregnancy: as pregnancy progresses, uterine vector displacement becomes more stable, periodic and organized, giving rise to better predictability, which is reflected in increased laminarity, determinism, maximum diagonal length and Shannon entropy. VMG recurrence statistics computed in the FWH outperformed those obtained in the FWL and the whole bandwidth, as well as classical temporal, spectral and non-linear parameters computed in the same FWH bandwidth in terms of the ability to discriminate between imminent and non-imminent labor and preterm and term labor. We also assessed the robustness of the proposed method against motion artifacts to preserve the ability to detect imminent labor and identify the preterm labor risk in TPL women. Our findings not only give a better understanding of uterine electrophysiology but would also provide clinical tools to better discriminate and prevent preterm labor in this group, thus improving maternal-fetal well-being and optimizing the management of hospital resources.

Ethical approval

The analysis of this database was approved by the Research Ethics Committee of the Faculty Research Ethics Panel (FREP) of Peking Union Medical College Hospital.

Consent to participate:

Informed consent was obtained from all individual participants included in the study.

Funding

This work was supported by the Spanish Ministry of Science and Innovation and the European Regional Development Fund, State Plan for Scientific, Technical and Innovation Research 2021–2023 (PID2021-124038OB-I00). This research was funded by the National Key R&D Program, grant number 2019YFC0119700, and the National Natural Science Foundation of China, grant number U20A20388.

CRediT authorship contribution statement

Felix Nieto-del-Amor: Conceptualization, Methodology, Software, Investigation, Validation, Formal analysis, Writing – original draft, Writing – review & editing. **Gema Prats-Boluda:** Conceptualization, Methodology, Investigation, Validation, Writing – review & editing, Supervision, Funding acquisition, Project administration. **Wanting Li:** Resources, Data curation, Methodology, Software, Writing – original draft, Writing – review & editing. **Jose L. Martinez-de-Juan:** Writing – original draft, Validation, Writing – review & editing. **Lin Yang:** Resources, Data curation, Writing – review & editing. **Yongxiu Yang:** Resources, Data curation, Writing – review & editing. **Dongmei Hao:** Conceptualization, Methodology, Investigation, Validation, Resources, Writing – review & editing, Supervision, Funding acquisition, Project administration. **Yiyao Ye-Lin:** Conceptualization, Methodology, Investigation, Validation, Writing – review & editing, Supervision, Funding acquisition, Project administration.

Declaration of Competing Interest

The authors declare that they have no known competing financial interests or personal relationships that could have appeared to influence the work reported in this paper.

Data availability

The data that has been used is confidential.

Appendix A

This appendix details how X2-Y2 was chosen as the best VMG configuration. We compared the ability of the different VMG configurations to detect preterm and imminent labor in women with TPL by assessing the number of statistics with statistically significant differences between groups (see Table A.1) and inter-group separability. Fig. A.1 and Fig. A.2 show the box and whisker plot of the four recurrence statistics of the different configurations to distinguish between imminent and non-imminent labor, preterm and term labor, respectively, with their corresponding p-value and Cohen's effect size (d value above each subplot).

Four statistics were computed for each VMG configuration in 3 different bandwidths (WBW, FWL and FWH): determinism (DET), longest diagonal (L_{max}), entropy (ENTR), and laminarity (LAM), giving rise to 12 comparisons between the groups (imminent vs. non-imminent, preterm vs. term). We counted the number of statistics of all the VMG configurations that showed significant changes between the groups ($\alpha = 0.05$).

We then found that X1-Y1 and X2-Y2 performed equally well in terms of $\Sigma(p < 0.05)$, specifically, 38 for X1-Y1 compared to 39 for X2-Y2, although X2-Y2 achieved lower p-values and higher Cohen's d effect size than X1-Y1. We therefore finally chose X2-Y2 as the best configuration.

References

[1] S. Chawanpaiboon, J.P. Vogel, A.B. Moller, P. Lumbiganon, M. Petzold, D. Hogan, S. Landoulsi, N. Jampathong, K. Kongwattanakul, M. Laopaiboon, et al., Global, regional, and national estimates of levels of preterm birth in 2014: A systematic review and modelling analysis, Lancet Glob. Heal. 7 (2019) e37–e46, https://doi.org/10.1016/S2214-109X(18)30451-0.

[2] C.P. Howson, M.V. Kinney, L. McDougall, J.E. Lawn, Born too soon: preterm birth matters, Reprod. Health 10 (2013) 1–9, https://doi.org/10.1186/1742-4755-10-S1-S1.

[3] C.S.H. Aarnoudse-Moens, N. Weisglas-Kuperus, J.B. Van Goudoever, J. Oosterlaan, Meta-analysis of neurobehavioral outcomes in very preterm and/or very low birth weight children, Pediatrics 124 (2009) 717–728, https://doi.org/10.1542/peds.2008-2816.

[4] N.J. Waitzman, A. Jalali, S.D. Grosse, Preterm birth lifetime costs in the United States in 2016: An update, Semin. Perinatol. 45 (2021), 151390, https://doi.org/10.1016/j.semperi.2021.151390.

[5] C. Paules, V. Pueyo, E. Martí, S. de Vilchez, I. Burd, P. Calvo, D. Oros, Threatened preterm labor is a risk factor for impaired cognitive development in early childhood, Am. J. Obstet. Gynecol. 216 (157) (2017) e1–157.e7, https://doi.org/10.1016/j.ajog.2016.10.022.

[6] A. Lavie, N. Czuzoj-Shulman, A.R. Spence, J. Barrett, H.A. Abenhaim, Hospital antenatal admissions for threatened preterm labor: how long should we be "Observing"? Arch. Gynecol. Obstet. 305 (2022) 31–37, https://doi.org/10.1007/s00404-021-06106-7.

[7] N. Wk, F. Kd, P. Nr, Economic burden of hospitalizations for preterm labor in the United States, Obstet. Gynecol. 96 (2000) 95–101, https://doi.org/10.1016/S0029-7844(00)00863-2.

[8] M. Lucovnik, L.R. Chambliss, R.E. Garfield, Costs of unnecessary admissions and treatments for "threatened preterm labor", Am. J. Obstet. Gynecol. 209 (217) (2013) e1–217.e3, https://doi.org/10.1016/j.ajog.2013.06.046.

[9] M.L. McPheeters, W.C. Miller, K.E. Hartmann, D.A. Savitz, J.S. Kaufman, J. M. Garrett, J.M. Thorp, The epidemiology of threatened preterm labor: A prospective cohort study, Am. J. Obstet. Gynecol. 192 (2005) 1325–1329, https://doi.org/10.1016/j.ajog.2004.12.055.

[10] J. Mas-Cabo, G. Prats-Boluda, J. Garcia-Casado, J. Alberola-Rubio, R. Monfort-Ortiz, C. Martinez-Saez, A. Perales, Y. Ye-Lin, Electrohysterogram for ANN-based prediction of imminent labor in women with threatened preterm labor undergoing tocolytic therapy, Sensors 20 (2020) 2681, https://doi.org/10.3390/s20092681.

[11] A. Lemancewicz, M. Borowska, P. Kuć, E. Jasińska, P. Laudański, T. Laudański, E. Oczeretko, Early diagnosis of threatened premature labor by electrohysterographic recordings - the use of digital signal processing, Biocybern. Biomed. Eng. 36 (2016) 302–307, https://doi.org/10.1016/j.bbe.2015.11.005.

[12] M. Albaladejo-Belmonte, G. Prats-Boluda, Y. Ye-Lin, R.E. Garfield, J. Garcia-Casado, Uterine slow wave: directionality and changes with imminent delivery, Physiol. Meas. (2022) 43, https://doi.org/10.1088/1361-6579/ac84c0.

[13] T. Desplanches, C. Lejeune, J. Cottenet, P. Sagot, C. Quantin, Cost-effectiveness of diagnostic tests for threatened preterm labor in singleton pregnancy in France, Cost Eff. Resour. Alloc. 16 (2018) 21, https://doi.org/10.1186/S12962-018-0106-Y.

[14] A. Leaños-Miranda, A.G. Nolasco-Leaños, R.I. Carrillo-Juárez, C.J. Molina-Pérez, I. Isordia-Salas, K.L. Ramírez-Valenzuela, Interleukin-6 in amniotic fluid: A reliable marker for adverse outcomes in women in preterm labor and intact membranes, Fetal Diagn. Ther. 48 (2021) 313–320, https://doi.org/10.1159/000514898.

[15] J. Garcia-Casado, Y. Ye-Lin, G. Prats-Boluda, J. Mas-Cabo, J. Alberola-Rubio, A. Perales, Electrohysterography in the diagnosis of preterm birth: A review, Physiol. Meas. 39 (2018) 02TR01, https://doi.org/10.1088/1361-6579/aaad56.

[16] M. Sean Esplin, M.A. Elovitz, J.D. Iams, C.B. Parker, R.J. Wapner, W.A. Grobman, H.N. Simhan, D.A. Wing, D.M. Haas, R.M. Silver, et al., Predictive accuracy of serial transvaginal cervical lengths and quantitative vaginal fetal fibronectin levels for spontaneous preterm birth among nulliparous women, Obstet. Gynecol. Surv. 72 (2017) 397–399, https://doi.org/10.1097/OGX.0000000000000455.

[17] D. Devedeux, C. Marque, S. Mansour, G. Germain, J. Duchêne, Uterine electromyography: A critical review, Am. J. Obstet. Gynecol. 169 (1993) 1636–1653, https://doi.org/10.1016/0002-9378(93)90456-S.

[18] G. Fele-Žorž, G. Kavšek, Ž. Novak-Antolič, F. Jager, A comparison of various linear and non-linear signal processing techniques to separate uterine EMG records of term and pre-term delivery groups, Med. Biol. Eng. Comput. 46 (2008) 911–922, https://doi.org/10.1007/s11517-008-0350-y.

[19] R.E. Garfield, L. Murphy, K. Gray, B. Towe, Review and study of uterine bioelectrical waveforms and vector analysis to identify electrical and mechanosensitive transduction control mechanisms during labor in pregnant patients, Reprod. Sci. 28 (2021) 838–856, https://doi.org/10.1007/s43032-020-00358-5.

[20] F. Nieto-del-amor, R. Beskhani, Y. Ye-Lin, J. Garcia-Casado, A. Diaz-Martinez, Assessment of dispersion and bubble entropy measures for enhancing preterm birth prediction based on electrohysterographic signals, Sensors 21 (2021), https://doi.org/10.3390/s21186071.

[21] F. Nieto-del-Amor, G. Prats-Boluda, J. Garcia-Casado, A. Diaz-Martinez, V.J. Diago-Almela, R. Monfort-Ortiz, D. Hao, Y. Ye-Lin, Combination of feature selection and resampling methods to predict preterm birth based on electrohysterographic signals from imbalance data, Sensors 22 (2022) 5098, https://doi.org/10.3390/s22145098.

[22] E. Mikkelsen, P. Johansen, A. Fuglsang-Frederiksen, N. Uldbjerg, Electrohysterography of labor contractions: propagation velocity and direction, Acta Obstet. Gynecol. Scand. 92 (2013) 1070–1078, https://doi.org/10.1111/aogs.12190.

[23] F. Jager, K. Geršak, P. Vouk, Ž. Pirnar, A. Trojner-Bregar, M. Lučovnik, A. Borovac, Assessing velocity and directionality of uterine electrical activity for preterm birth prediction using Ehg surface records, Sensors (switzerland) 20 (2020) 1–30.

[24] D.B. Escalona-Vargas Rathinaswamy Govindan, A.L. Furdea Pam Murphy Curtis Lowery, Characterizing the propagation of uterine electrophysiological signals recorded with a multi-sensor abdominal array in term pregnancies, PLoS One 10 (2015), 140894, https://doi.org/10.1371/journal.pone.0140894.

[25] M. Lingman, M. Hartford, T. Karlsson, J. Herlitz, A. Rubulis, K. Caidahl, L. Bergfeldt, Transient repolarization alterations dominate the initial phase of an acute anterior infarction - A vectorcardiography study, J. Electrocardiol. 47 (2014) 478–485, https://doi.org/10.1016/j.jelectrocard.2014.04.017.

[26] M. Sederholm, The origin of monitoring of acute myocardial infarction with continuous vectorcardiography, J. Electrocardiol. 47 (2014) 418–424, https://doi.org/10.1016/j.jelectrocard.2014.04.002.

[27] D. Cortez, J.M. Bos, M.J. Ackerman, Vectorcardiography identifies patients with electrocardiographically concealed long QT syndrome, Hear. Rhythm 14 (2017) 894–899, https://doi.org/10.1016/j.hrthm.2017.03.003.

[28] H. Yang, Multiscale recurrence quantification analysis of spatial cardiac vectorcardiogram signals, IEEE Trans. Biomed. Eng. 58 (2011) 339–347, https://doi.org/10.1109/TBME.2010.2063704.

[29] H. Zhang, C. Liu, F. Tang, M. Li, D. Zhang, L. Xia, N. Zhao, S. Li, S. Crozier, W. Xu, et al., Cardiac arrhythmia classification based on 3D recurrence plot analysis and deep learning, Front. Physiol. 13 (2022) 1–13, https://doi.org/10.3389/fphys.2022.956320.

[30] J. Iwaniec, M. Iwaniec, A. Kalukiewicz, Application of vectorcardiography and recurrence-based methods to analysis of ECG signals, MATEC Web Conf. 241 (2018) 4–7, https://doi.org/10.1051/matecconf/201824101015.

[31] J.P. Eckmann, O. Oliffson Kamphorst, D. Ruelle, Recurrence plots of dynamical systems, Epl 4 (1987) 973–977, https://doi.org/10.1209/0295-5075/4/9/004.

[32] N. Marwan, M. Carmen Romano, M. Thiel, J. Kurths, Recurrence plots for the analysis of complex systems, Phys. Rep. 438 (2007) 237–329, https://doi.org/10.1016/j.physrep.2006.11.001.

[33] H. Poincaré, Sur Le Problème Des Trois Corps et Les Équations de La Dynamique, Acta Math. 13 (1890) A3–A270.

[34] N. Marwan, N. Wessel, U. Meyerfeldt, A. Schirdewan, J. Kurths, Recurrence-plot-based measures of complexity and their application to heart-rate-variability data, Phys. Rev. E - Stat. Physics, Plasmas, Fluids, Relat. Interdiscip. Top. 66 (2002) 1–8, https://doi.org/10.1103/PhysRevE.66.026702.

[35] K. Zhao, H. Wen, Y. Guo, A. Scano, Z. Zhang, Feasibility of recurrence quantification analysis (RQA) in quantifying dynamical coordination among muscles, Biomed. Signal Process. Control 79 (2023), 104042, https://doi.org/10.1016/j.bspc.2022.104042.

[36] T. Heunis, C. Aldrich, J.M. Peters, S.S. Jeste, M. Sahin, C. Scheffer, P.J. de Vries, Recurrence quantification analysis of resting state EEG signals in autism spectrum disorder - a systematic methodological exploration of technical and demographic confounders in the search for biomarkers, BMC Med. 16 (2018) 1–17, https://doi.org/10.1186/s12916-018-1086-7.

[37] M. Borowska, E. Brzozowska, P. Kuć, E. Oczeretko, R. Mosdorf, P. Laudański, Identification of preterm birth based on RQA analysis of electrohysterograms, Comput. Methods Programs Biomed. 153 (2018) 227–236, https://doi.org/10.1016/j.cmpb.2017.10.018.

[38] D. Hao, J. Peng, Y. Wang, J. Liu, X. Zhou, D. Zheng, Evaluation of convolutional neural network for recognizing uterine contractions with electrohysterogram, Comput. Biol. Med. 113 (2019), 103394, https://doi.org/10.1016/j.compbiomed.2019.103394.

[39] J. Xu, Z. Chen, H. Lou, G. Shen, A. Pumir, Review on EHG signal analysis and its application in preterm diagnosis, Biomed. Signal Process. Control 71 (2022) 1–18, https://doi.org/10.1016/j.bspc.2021.103231.

[40] Y. Ye-Lin, J. Garcia-Casado, G. Prats-Boluda, J. Alberola-Rubio, A. Perales, Automatic identification of motion artifacts in EHG recording for robust analysis of uterine contractions, Comput. Math. Methods Med. 2014 (2014), https://doi.org/10.1155/2014/470786.

[41] J. Peng, D. Hao, L. Yang, M. Du, X. Song, H. Jiang, Y. Zhang, D. Zheng, Evaluation of electrohysterogram measured from different gestational weeks for recognizing preterm delivery: A preliminary study using random forest, Biocybern. Biomed. Eng. 40 (2020) 352–362, https://doi.org/10.1016/j.bbe.2019.12.003.

[42] P. Fergus, I. Idowu, A. Hussain, C. Dobbins, Advanced artificial neural network classification for detecting preterm births using EHG records, Neurocomputing 188 (2016) 42–49, https://doi.org/10.1016/j.neucom.2015.01.107.

[43] A. Smrdel, F. Jager, Separating sets of term and pre-term uterine EMG records, Physiol. Meas. 36 (2015) 341–355, https://doi.org/10.1088/0967-3334/36/2/341.

[44] P. Fergus, P. Cheung, A. Hussain, D. Al-Jumeily, C. Dobbins, S. Iram, Prediction of preterm deliveries from EHG signals using machine learning, PLoS One 8 (2013) e77154.

[45] P. Ren, S. Yao, J. Li, P.A. Valdes-Sosa, K.M. Kendrick, Improved prediction of preterm delivery using empirical mode decomposition analysis of uterine electromyography signals, PLoS One 10 (2015) e0132116.

[46] U.R. Acharya, V.K. Sudarshan, S.Q. Rong, Z. Tan, C.M. Lim, J.E. Koh, S. Nayak, S. V. Bhandary, Automated detection of premature delivery using empirical mode and wavelet packet decomposition techniques with uterine electromyogram signals, Comput. Biol. Med. 85 (2017) 33–42, https://doi.org/10.1016/j.compbiomed.2017.04.013.

[47] M.U. Ahmed, T. Chanwimalueang, S. Thayyil, D.P. Mandic, A multivariate multiscale fuzzy entropy algorithm with application to uterine EMG complexity analysis, Entropy 19 (2017) 2, https://doi.org/10.3390/e19010002.

[48] D. Radomski, A. Grzanka, S. Graczyk, A. Przelaskowski, Assessment of uterine contractile activity during a pregnancy based on a nonlinear analysis of the uterine electromyographic signal, Adv. Soft Comput. 47 (2008) 325–331, https://doi.org/10.1007/978-3-540-68168-7_37.

[49] R. Veerabhadrappa, I.T. Hettiarachchi, A. Bhatti, Using recurrence quantification analysis to quantify the physiological synchrony in dyadic ECG data, 15th Annu. IEEE Int. Syst. Conf. Syscon 2021 - Proc. (2021), https://doi.org/10.1109/SysCon48628.2021.9447059.

[50] C. Letellier, Estimating the Shannon entropy: recurrence plots versus symbolic dynamics, Phys. Rev. Lett. 96 (2006) 1–4, https://doi.org/10.1103/PhysRevLett.96.254102.

[51] J.P. Zbilut, N. Thomasson, C.L. Webber, Recurrence quantification analysis as a tool for nonlinear exploration of nonstationary cardiac signals, Med. Eng. Phys. 24 (2002) 53–60, https://doi.org/10.1016/S1350-4533(01)00112-6.

[52] L.Y. Di Marco, C. Di Maria, W.C. Tong, M.J. Taggart, S.C. Robson, P. Langley, Recurring patterns in stationary intervals of abdominal uterine electromyograms during gestation, Med. Biol. Eng. Comput. 52 (2014) 707–716, https://doi.org/10.1007/s11517-014-1174-6.

[53] S.S. Sawilowsky, New effect size rules of thumb, J. Mod. Appl. Stat. Methods 8 (2009) 597–599, https://doi.org/10.22237/jmasm/1257035100.

[54] J. Mas-Cabo, Y. Ye-Lin, J. Garcia-Casado, A. Díaz-Martinez, A. Perales-Marin, R. Monfort-Ortiz, A. Roca-Prats, Á. López-Corral, G. Prats-Boluda, Robust characterization of the uterine myoelectrical activity in different obstetric scenarios, Entropy 22 (2020) 743, https://doi.org/10.3390/e22070743.

[55] J. Mas-Cabo, G. Prats-Boluda, A. Perales, J. Garcia-Casado, J. Alberola-Rubio, Y. Ye-Lin, Uterine electromyography for discrimination of labor imminence in women with threatened preterm labor under tocolytic treatment, Med. Biol. Eng. Comput. 57 (2019) 401–411, https://doi.org/10.1007/s11517-018-1888-y.

[56] C. Ramon, H. Preissl, P. Murphy, J.D. Wilson, C. Lowery, H. Eswaran, Synchronization analysis of the uterine magnetic activity during contractions, Biomed. Eng. Online 4 (2005) 1–12, https://doi.org/10.1186/1475-925X-4-55.

[57] R.K. Riemer, M.A. Heymann, Regulation of uterine smooth muscle function during gestation, Pediatr. Res. 44 (1998) 615–627.

[58] A. Diab, S. Boudaoud, B. Karlsson, C. Marque, Performance comparison of coupling-evaluation methods in discriminating between pregnancy and labor EHG signals, Comput. Biol. Med. 132 (2021), 104308, https://doi.org/10.1016/j.compbiomed.2021.104308.

[59] A. Diab, M. Hassan, C. Marque, B. Karlsson, Performance analysis of four nonlinearity analysis methods using a model with variable complexity and application to uterine EMG signals, Med. Eng. Phys. 36 (2014) 761–767, https://doi.org/10.1016/j.medengphy.2014.01.009.

[60] S.M. Pincus, Approximate entropy as a measure of system complexity, Proc. Natl. Acad. Sci. u. s. a. 88 (1991) 2297–2301, https://doi.org/10.1073/pnas.88.6.2297.

[61] A. Humeau-Heurtier, Evaluation of systems' irregularity and complexity: sample entropy, its derivatives, and their applications across scales and disciplines, Entropy 20 (2018) 794, https://doi.org/10.3390/e20100794.

[62] F. Jager, S. Libenšek, K. Geršak, Characterization and automatic classification of preterm and term uterine records, PLoS One 13 (2018) e0202125.

[63] N. Nader, S. Zahran, C. Marque, M. Hassan, M. Yochum, W. Falou, M. Khalil, Graph analysis of uterine networks using EHG source connectivity, Int. Conf. Adv. Biomed. Eng. ICABME (2017) 2017-Octob, https://doi.org/10.1109/ICABME.2017.8167554.

[64] D.A. Kenny, L. Mannetti, A. Pierro, S. Livi, D.A. Kashy, The statistical analysis of data from small groups, J. Personal. Social Psychol. 83 (2002) 126–137, https://doi.org/10.1037//0022-3514.83.1.126.

[65] A.R. Pérez-Riera, R. Barbosa-Barros, R. Daminello-Raimundo, L.C. de Abreu, K. Nikus, The vectorcardiogram and the main dromotropic disturbances, Curr. Cardiol. Rev. 17 (2020) 50–59, https://doi.org/10.2174/1573403x16666200810105504.

[66] T. Włodarczyk, S. Płotka, T. Szczepański, P. Rokita, N. Sochacki-Wójcicka, J. Wójcicki, M. Lipa, T. Trzciński, Machine learning methods for preterm birth prediction: A review, Electron. 10 (2021) 1–24, https://doi.org/10.3390/electronics10050586.

[67] G. Prats-Boluda, J. Pastor-Tronch, J. Garcia-Casado, R. Monfort-Ortíz, A. Perales Marín, V. Diago, A. Roca Prats, Y. Ye-Lin, Optimization of imminent labor prediction systems in women with threatened preterm labor based on electrohysterography, Sensors 21 (2021) 1–18, https://doi.org/10.3390/s21072496.

[68] F. Nieto-del-Amor, G. Prats-Boluda, J.L. Martinez-De-Juan, A. Diaz-Martinez, R. Monfort-Ortiz, V.J. Diago-Almela, Y. Ye-Lin, Optimized feature subset selection using genetic algorithm for preterm labor prediction based on electrohysterography, Sensors 21 (2021) 3350, https://doi.org/10.3390/s21103350.

[69] T. Murphy Goodwin, L. Millar, L. North, L.S. Abrams, R.C. Weglein, M.L. Holland, The pharmacokinetics of the oxytocin antagonist atosiban in pregnant women with preterm uterine contractions, Am. J. Obstet. Gynecol. 173 (1995) 913–917, https://doi.org/10.1016/0002-9378(95)90365-8.

[70] U. Buscher, F.-C.-K. Chen, E. Riesenkampff, D. von Dehn, M.D.J.W. David, Effects of oxytocin receptor antagonist atosiban on pregnant myometrium in Vitro, Obstet. Gynecol. 98 (2001) 117–121.

[71] J. Mas-Cabo, G. Prats-Boluda, Y. Ye-Lin, J. Alberola-Rubio, A. Perales, J. Garcia-Casado, Characterization of the effects of atosiban on uterine electromyograms recorded in women with threatened preterm labor, Biomed. Signal Process. Control 52 (2019) 198–205, https://doi.org/10.1016/j.bspc.2019.04.001.

[72] R.B. Tambling, S.R. Anderson, *Statistical Analysis with Small Samples*; 2013; ISBN 9781136192203.

[73] M. Thiel, M.C. Romano, J. Kurths, R. Meucci, E. Allaria, F.T. Arecchi, Influence of observational noise on the recurrence quantification analysis, Phys. D Nonlinear Phenom. 171 (2002) 138–152, https://doi.org/10.1016/S0167-2789(02)00586-9.

[74] V. Mitra, A. Sarma, M.S. Janaki, A.N. Sekar Iyenger, B. Sarma, N. Marwan, J. Kurths, P.K. Shaw, D. Saha, S. Ghosh, Order to chaos transition studies in a DC glow discharge plasma by using recurrence quantification analysis, Chaos, Solitons and Fractals 69 (2014) 285–293, https://doi.org/10.1016/j.chaos.2014.10.005.

[75] C.L. Webber, J.P. Zbilut, Dynamical assessment of physiological systems and states using recurrence plot strategies, J. Appl. Physiol. 76 (1994) 965–973, https://doi.org/10.1152/jappl.1994.76.2.965.

[76] F. Esgalhado, A.G. Batista, H. Mouriño, S. Russo, C.R. Palma Dos Reis, F. Serrano, V. Vassilenko, M.D. Ortigueira, Automatic contraction detection using uterine electromyography, Appl. Sci. 10 (2020) 1–14, https://doi.org/10.3390/app10207014.